Improving Dynamic Response of Active Harmonic Compensator Using Digital Comb Filter

Muhammad Tahir, *Member, IEEE*, and Sudip K. Mazumder, *Senior Member, IEEE*

***Abstract*— Harmonic extraction and control is one of the main elements in active power filter design. The advances in the digital signal processor (DSP)-based control have facilitated the use of sophisticated filters and control techniques to achieve better dynamic performance, which was difficult earlier with the use of analog design. To improve the dynamic response of the active harmonic controller, we propose a *comb-filter*-based solution, which can be implemented on a DSP platform. Performance evaluation results for the load transient show a substantial improvement in the dynamic performance of the harmonic compensator compared with the conventional low-pass-filter-based approaches.**

***Index Terms*— Active power filter, comb filter, dynamic response, harmonic compensation.**

I. Introduction

THE need for power quality improvement is not new. Many power electronics systems, such as switching power electronics, passive diode rectifiers, thyristor-controlled loads, lead to harmonic generation and degrade the power quality significantly. Among those switching power electronics-based systems including uninterruptable switching power supplies, adjustable motor speed drives, energy-efficient lighting appliances, and inverters in power generation systems for distributed renewable-energy sources including, solar systems, wind turbines as well as fuel cells are one of the main sources of power quality degradation. High harmonic currents are one of the main contributors to the degraded power quality. Active power filters provide a means for improving the power quality in power distribution networks and the harmonic compensator is an integral part of active power filtering [1]. Fig. 1 shows the block diagram of a shunt harmonic compensator. One of the primary objectives of harmonic compensator is to generate a reference signal, which is used by the controller to eliminate the harmonic components present in the system. To extract the reference harmonic current from the load, instantaneous reactive power theory as well as synchronous reference frame has been used in [2] and [3].

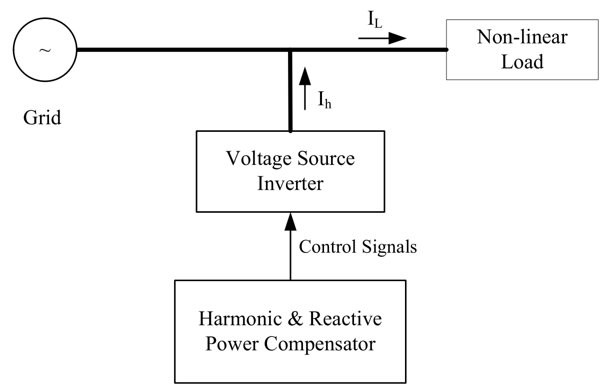

Fig. 1. System block diagram.

Resonant current control has also been used widely for reducing the current harmonic distortion in many different distributed generation applications [4], [5]. A resonant harmonic compensator attenuates the current harmonics and is capable of achieving zero steady-state error. However, resonant compensator suffers performance deterioration caused by abnormal grid condition. This issue is partly addressed using phase-locked loop-based solutions to generate reference signals, which are not affected by harmonics, interharmonics as well as load imbalances [6]. In addition, resonant compensator does not provide good transient performance and has limitations related to digital implementation [7].

The synchronous reference frame, based on abc to dq0 transformation, has also been widely adopted in harmonic compensation. This method has the advantage of converting the harmonics of interest to a dc component so that each of the harmonics can be processed independently with zero steady-state errors [8]. In addition, this method allows the use of different types of filters in the design of harmonic compensator. Since the remaining harmonics present in the signal, in abc to dq0 transformation, are mapped to other harmonics, which are required to be eliminated before this signal can be fed to the controller. The natural choice to reject these unwanted harmonics is to employ the low-pass filter, which retains only the dc component corresponding to a particular harmonic and reject all of the frequency components caused by other harmonics. This requires choosing a filter of higher order and lower cutoff frequency for better steady-state performance. But, the presence of this low-pass filter significantly degrades the dynamic performance of the harmonic compensator block. This leads to large settling times in case of a load transient. Tolbert *et al.* [9] have shown that with a lower cutoff frequency

Manuscript received January 18, 2014; revised May 20, 2014 and July 18, 2014; accepted August 1, 2014. Date of publication August 6, 2014; date of current version October 29, 2014. This work was supported in part by the U.S. National Science Foundation (NSF) under Award 1239118, received by Prof. Mazumder in the year 2012. However, any opinions, findings, conclusions, or recommendations expressed herein are those of the authors and do not necessarily reflect the views of the NSF. Recommended for publication by Associate Editor M. Molinas.

M. Tahir is with the Department of Electrical Engineering, University of Engineering and Technology Lahore, Lahore 54890, Pakistan (e-mail: mtahir@uet.edu.pk).

S. K. Mazumder is with the Department of Electrical and Computer Engineering, University of Illinois at Chicago, Chicago, IL 60607 USA (e-mail: mazumder@ece.uic.edu).

Color versions of one or more of the figures in this paper are available online at http://ieeexplore.ieee.org.

Digital Object Identifier 10.1109/JESTPE.2014.2345741

of the low-pass filter, more of the active power ripple is filtered at the expense of an extended response time to step changes in the load current. The results in [9] show that with a 5 Hz cutoff frequency, the response time to step change is approximately 1.5 line cycles at 60 Hz and active power ripple more than 90% is filtered.

Different control techniques have been proposed to improve the dynamic response of the active power compensator [10]–[12]. In [10], an all-digital repetitive plug-in controller for odd-harmonics is used for the current control loops of the active filter, which uses a low-pass finite-impulse-response filter in the feedback path. Active power balance for the whole system is achieved by an outer control loop designed from an energy-balancing perspective. Rahmani *et al.* [11] have presented a nonlinear control for a three-phase shunt hybrid power filter to enhance the dynamic response when employed to compensate for harmonic currents and reactive power. Two inner current dynamic loops and a dc-voltage outer loop using PI controllers provide the reactive power and harmonic currents required by the nonlinear load. An integrated digital implementation of control algorithm and the required signal processing for active power filter is proposed in [12]. The solution proposed uses a fourth order infinite-impulse-response low-pass filter with 60 Hz cutoff frequency to attenuate the harmonic components. In all the aforementioned controller solutions, the use of low-pass digital filters with small bandwidth, on the order of fundamental frequency, in the feedback path is the main reason for limited dynamic response.

To overcome the issue of limited bandwidth and to improve the dynamic performance of the active harmonic compensator, we propose a reconfigurable solution using digital comb filter. The proposed solution improves the transient response significantly and can be implemented using a digital signal processor (DSP). In addition, the proposed solution is capable of dynamically adapting the filter sampling frequency to align the notch frequencies of the comb filter with the harmonic frequencies allowing to track any frequency variations in the load current. Rest of the paper is organized as follows.

In Section II, we describe the details of conventional and modified comb filter design. In addition, the comb filter dynamic performance is evaluation in this section. The design of active harmonic compensator is discussed in Section III. The performance evaluation results showing the improvement in the dynamic response are provided in Section IV. Finally, we conclude our findings in Section V.

II. Comb Filter Design

A conventional digital comb filter has the following z-domain system transfer function [13]:

$$H(z) = \frac{1}{M}\frac{1 - z^{-M}}{1 - z^{-1}} \tag{1}$$

where M is the order of the filter. The expression in (1) can be rewritten as

$$H(z) = \frac{1}{M}\frac{z^M - 1}{z^M}\frac{z}{z - 1}. \tag{2}$$

From the transfer function expression in (2), it can be observed that the zeros of the filter are on the unit circle and all the poles are at origin of the z-plane. The expression in (2), first modified to pole-zero form and then using the substitution $z = e^{j\omega}$ becomes

$$\begin{aligned} H(z) &= \frac{1}{M}\prod_{k'=1}^{M}\frac{z - z_{k'}}{z - p_{k'}} \\ &= \frac{1}{M}\prod_{k'=1}^{M}\frac{e^{j\omega} - z_{k'}}{e^{j\omega} - p_{k'}}. \end{aligned} \tag{3}$$

From the second expression in (3), it can be observed that for some $\omega = \omega_i$ we will have $e^{j\omega_i} = z_i$ and the magnitude response at that frequency results in zero output. This ideal scenario of zero output at different $\omega_i, i \in \{1, 2, \ldots, M\}$ is equivalent to having an infinite attenuation at those frequencies, which we call the notch frequencies of the comb filter. The notch frequencies are integer multiples of the fundamental frequency.

Ideally, the conventional comb filter provides zero gain at notch frequencies and variable gain in the passband and no effects on the phase of the signal in the passband [13]. These characteristics, almost unachievable using analog implementation, can be closely matched using a practical digital implementation, as we describe in this section.

The conventional comb filter discussed above practically provides large attenuation at the selected notch frequencies, but its passband attenuation is different at different frequencies. Now we introduce a modified version of the comb filter [14] that can provide almost flat gain in the passband. However, this is achieved by moving the poles away from the origin toward unit circle and the pole frequencies are the same as that of zeros. The modified comb filter transfer function is given by

$$H_m(z) = \frac{1 - z^{-M}}{1 - z^{-1}}\frac{1 - \mathrm{rz}^{-1}}{1 - (\mathrm{rz}^{-1})^M} \tag{4}$$

$$= \prod_{k=1}^{M+1}\frac{z - z_k}{z - p_k} \tag{5}$$

where the parameter $r \in [0, 1)$ is the attenuation factor of comb filter at the notch frequencies. The attenuation factor r equal to 0 reduces the modified comb filter to the original conventional comb filter of (1). On the other extreme, for $r = 1$ the comb filter becomes an all-pass filter. In (4), the pole-zero locations are determined by

$$\begin{aligned} z_k &= e^{j2\pi\frac{k}{M+1}f_s} \\ p_k &= \mathrm{r}e^{j2\pi\frac{k}{M+1}f_s}. \end{aligned} \tag{6}$$

In (6), f_s is the sampling frequency and is related to pole-zero frequencies by

$$f_{z_k} = f_{p_k} = k\frac{f_s}{M + 1}. \tag{7}$$

The frequency response of the filter is normalized by the filter dc gain, K_c and substituting z with $e^{j\omega}$ is given by

$$H_m(e^{j\omega}) = \frac{(e^{j\omega} - z_1)(e^{j\omega} - z_2)\ldots(e^{j\omega} - z_{M+1})}{(e^{j\omega} - p_1)(e^{j\omega} - p_2)\ldots(e^{j\omega} - p_{M+1})}. \tag{8}$$

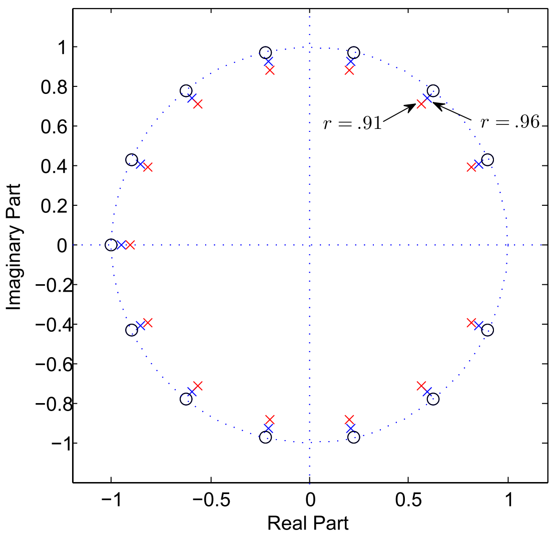

(a)

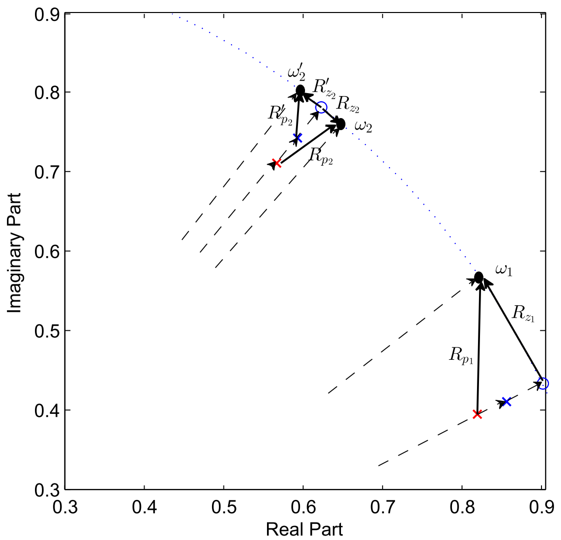

(b)

Fig. 2. (a) z-Plane pole (marked as x) and zero (marked as o) plot for the comb filter with $M = 14$ and two different values of the parameter r. (b) Magnified section of pole-zero plot to illustrate the dependency of comb filter attenuation on the parameter r.

The dc gain, K_c in (8) is obtained as

$$K_c = \prod_{i=1}^{M} \frac{R_{p_i}}{R_{z_i}}$$

where $R_{p_i} = |1 - p_i|$ and $R_{z_i} = |1 - z_i|$. In (8), a pole-zero pair is located at $1\angle 0^o$ and should be canceled before the evaluation of dc gain.

Fig. 2(a) shows the pole-zero plots of the comb filter, for two different values of the attenuation factor r, with notch frequencies spanning from the fundamental to the seventh harmonic. For the plot shown in Fig. 2(a), pole-zero pairs lying in the upper half of the z-plane are mapped to real frequencies in the f domain. To place the first pole-zero pair at the fundamental frequency and to design the comb filter that can remove up to seventh harmonic, the required sampling frequency for filter order $M = 14$ is obtained by using (7) and is given by $f_s = M/kf_{p_k} = 840$ Hz, where $k = 1$ and $f_{p1} = 60$ Hz. The result shown in Fig. 2(b) is the magnified version of the pole-zero plot shown in Fig. 2(a). This result will be used to explain the dependency of the comb filter attenuation on the value of parameter r.

From the frequency transfer function expression in (8) for the comb filter, let us consider two pole-zero pairs for illustration purpose. The term $|e^{j\omega_1} - z_1|$ represent the vector difference between the two vectors (shown as dotted arrows) drawn from the origin to the unit circle at points ω_1 and z_1 and is denoted as R_{z_1}. Similarly, the corresponding denominator term $|e^{j\omega_1} - p_1|$ also represent the difference between the pole p_1 and the unit vector at ω_1 and is denoted by R_{p_1}. The vectors R_{z_1} and R_{p_1} can observed from Fig. 2(b), where they are shown as solid arrows. The ratio R_{z_1}/R_{p_1} is approximately equal to one. Next, we choose ω_2 and ω_2' in the close proximity of the second pole-zero pair. For this case, we observe that R_{z2}/R_{p2} is smaller than R'_{z2}/R'_{p2}, because R'_{p2} is smaller than R_{p2}. The corresponding value of parameter r is smaller for R_{p2} than that of R'_{p2} illustrating the reason for higher attenuation at lower values of parameter r.

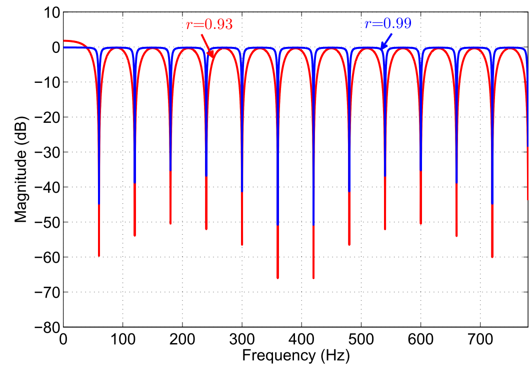

(a)

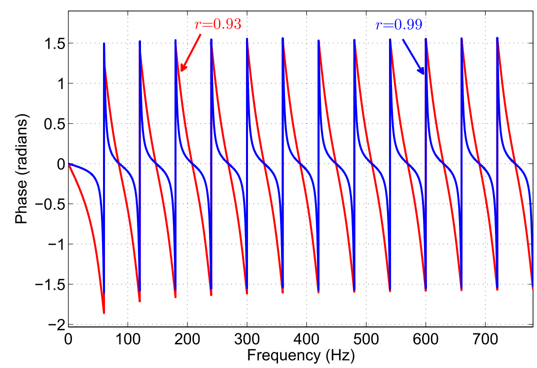

(b)

Fig. 3. Comb filter response for (a) magnitude and (b) phase for two different values of the parameter r.

Fig. 3 shows the magnitude and phase responses of the digital comb filter for two different values of the parameter r. It can be observed that the 3 dB bandwidth at notch frequencies decreases with an increase in the attenuation factor, r, providing an improved flat response in the passband.

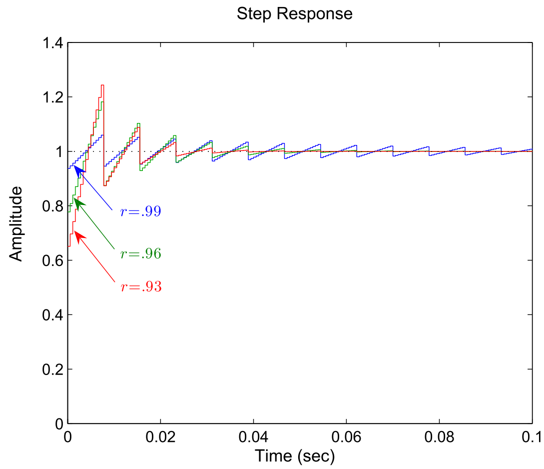

Fig. 4. Step response performance of comb filter for different values of parameter r. Filter order, $M = 14$, is used for this response.

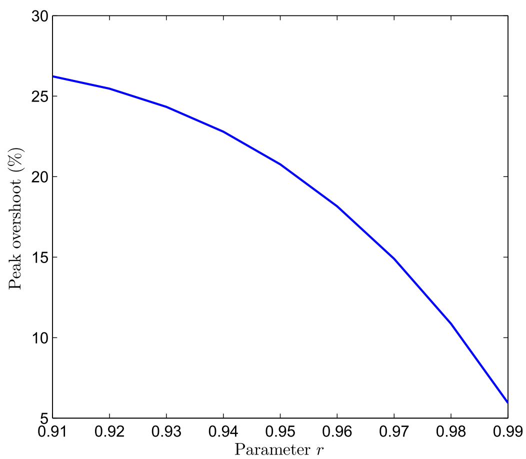

Fig. 5. Percentage overshoot performance of comb filter for different values of parameter r. $M = 14$ for this response.

However, the attenuation at the notch frequencies reduces with an increase in the parameter r as discussed above. This underlying performance tradeoff between the achievable attenuation at the notch frequencies and the 3 dB bandwidth (as well as flatness of the frequency response in the passband) can be tuned by choosing an appropriate value of parameter r. One possible solution to the optimal choice of parameter r can be obtained by minimizing the filter gain-bandwidth product at the notch frequencies.

The step response of comb filter for different values of attenuation factor is shown in Fig. 4. We observe that decreasing parameter r results in an increase in the overshoot, but the corresponding settling time is reduced. In addition, it is also observed that the filter rise time does not change when parameter r changes. The overshoot and settling time performance for step input as a function of parameter r is shown in Figs. 5 and 6, respectively. In a conventional filter step response, an increase in the overshoot also leads to an increase in the settling time. However, from the step response of digital comb filter for the selected range of parameter r, we observe that an increase in overshoot is accompanied by a

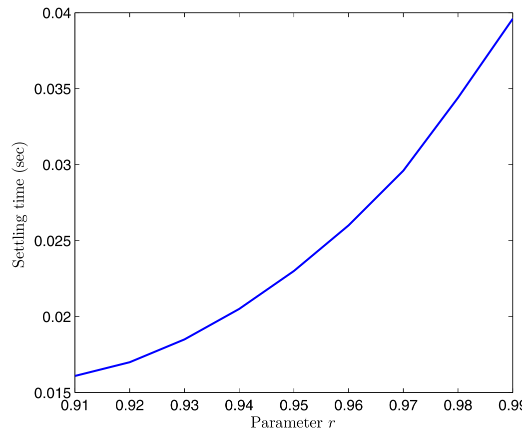

Fig. 6. Settling time performance of comb filter for different values of parameter r. Filter order, $M = 14$, is used for this response.

corresponding decrease in the settling time as can be observed from the result in Figs. 5 and 6.

In the digital implementation, the maximum value of r is limited by the resolution supported by the processor. There is a tradeoff, in the design of the comb filter, between the value of r and the order M of the filter and is contingent to the performance requirement. Higher order of the filter requires more memory, but owing to the exponential decrease of the factor r^M, the filter can be implemented using a lower-resolution processing unit. Hence, there is a compromise between the order of the filter and processing unit resolution. A simple design procedure for realizing the filter is outlined in [15]. The parameter r of the comb filter is selected to obtain the desired attenuation at the line frequency and at frequencies multiples of the line frequency.

From practical realization viewpoint, the use of delta transform is capable of providing more accurate implementation and can be easily incorporated using the available mapping from z-transform to δ-transform. Let $y(k\Delta)$ represent the discrete time sampled signal, where k is time index and Δ is the sample time. Now if $Y(z)$ and $Y(\delta)$ represent the z and delta-transforms, respectively, then we have $Y(\delta) = \Delta Y(z)\,|_{z=\Delta\delta+1}$. This mapping can be used to transform the z-domain comb filter to its δ-domain counterpart.

III. Compensator Design and Sampling Frequency Adaptation

In this section, we discuss the compensator design for both the harmonic filtering and the reactive power compensation. In addition, frequency adaptation for harmonic compensation to follow any arbitrary frequency variations is also discussed.

A. Active Compensator Design

The overall control system comprise of a multiloop structure, where the voltage outer loop is responsible for maintaining the dc capacitor voltage (V_{dc}) to a set reference value of V_{ref}. The output of the voltage controller is fed to current compensator and it acts as a reference for the d component

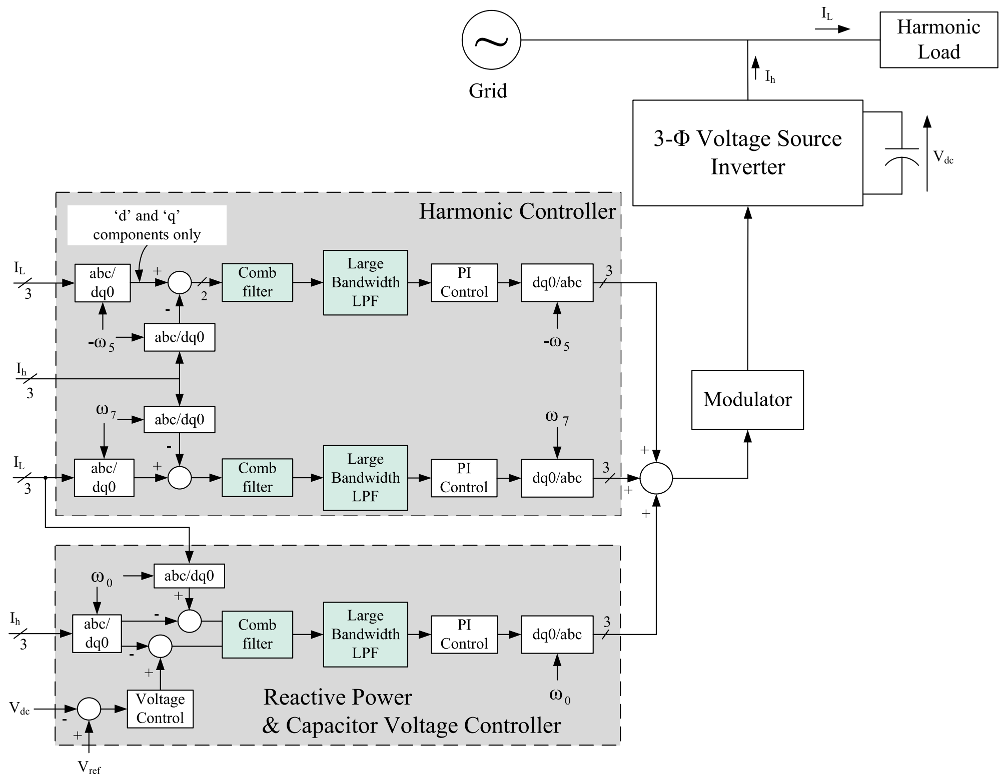

Fig. 7. Harmonic controller structure with the *comb filter* replacing the low-pass filter. Numeral 3 represents three phases. Balanced load is used which has only d and q nonzero components.

of the fundamental current control. The reactive power compensation is also implemented using the q component of the current at fundamental frequency as can be observed from reactive power and capacitor voltage subblock shown in Fig. 7. Fig. 7 also shows the system block diagram for the harmonic compensator designed, for fifth and seventh harmonics, by replacing the conventional narrow band low-pass filter with the combination of digital comb filter and a large bandwidth low-pass filter.

In synchronous reference frame control, after performing abc–dq0 transformation, as shown in Fig. 7, the error-signal is obtained by subtracting the harmonic compensator feedback from the load current. This error-signal is then passed through a comb filter to remove any high-frequency components and is applied to the PI compensator. The output of each of the PI compensator is passed through the dq0–abc transformation and the resulting signals are added to generate the controller output used by the modulator to generate the pulse width-modulated signals to drive the switches.

For performance comparison we used a diode rectifier type of three-phase nonlinear load for which the harmonics generated are given by $6n \pm 1$ for $n = \{1, 2, \ldots\}$, where $6n - 1$ are negative sequence and $6n + 1$ are positive sequence harmonics, respectively. Fig. 7 shows the controller structure only for fifth and seventh harmonics and can be extended for eliminating higher order harmonics depending on the performance and total harmonic distortion (THD) requirements. Use of the comb filter allows one to tune the PI controller gains to improve the dynamic performance. Same comb filter is used for all the harmonics and as a result simplifies the design procedure for harmonic compensator.

B. Sampling Frequency Adaptation

The frequencies ω_0, ω_5, and ω_7 used by the compensator, as shown in Fig. 7, are obtained from the load current. If the system frequency variations are ignored then the nominal fundamental frequency as well as harmonics can be generated locally. However, this can significantly degrade the comb-filter-based harmonic compensator performance in the presence of frequency deviations.

A variation in the sampling frequency to grid frequency ratio is equivalent to the case of having a fixed sampling frequency while the grid frequency has deviated. This will result in the deviation of comb filter notch frequencies, which in turn will lead to reduced attenuation of harmonics. Since any variation in the fundamental frequency will also change the harmonics frequency, sampling frequency adaptation is required for effective harmonic compensation.

The first step to address this issue is to acquire accurate frequency estimates of the fundamental as well as harmonics. For that purpose, the real-time fundamental and harmonic frequency estimates can be obtained using the solution in [16]. The proposed approach in [16] is based on parallel resonators with common feedback combined with an external Finite Impulse Response comb-filter-based module for frequency estimation. Another possible approach that can be used for real-time frequency estimation is proposed in [17].

Once accurate frequency estimate is obtained, the next step is to adapt the filter parameters, that is, poles and zeros frequencies using (7), which in turn requires adapting sampling frequency. Let f_0 denotes the estimated fundamental frequency and f_s is the instantaneous sampling frequency of the filter, then we have

$$f_s = M f_0. \quad (9)$$

Since harmonics are an integer multiple of the fundamental frequency, the parameter M is always an integer. However, it is worth mentioning that we are not considering the possibility of compensating any interharmonics. In digital implementation, the sampling frequency can be generated using a timer module. The timer reload (TR) value can be adjusted in real-time based on the current estimate of f_s. Assuming f_c is the clock frequency of the processor used for digital implementation, the TR value can be obtained by TR $= f_c/Mf_0$.

The ratio of sampling to fundamental frequency can be increased by modifying the expression in (9) as

$$\tilde{f}_s = l M f_0. \quad (10)$$

In (10), l is the sampling frequency improvement factor and $l \in \{1, 2, \ldots, \lfloor f_c/Mf_0 \rfloor\}$. A larger value of l will increase the actual sampling frequency, $\tilde{f}_s$, but the sampling frequency of comb filter is required to be f_s for its proper implementation. This can be achieved by averaging every l samples to construct one sample for the compensator. For this case, the TR value can be redefined as TR $= f_c/lMf_0$.

In the aforementioned approach, to increase the ratio of system sampling frequency to the fundamental frequency, any variation in fundamental frequency, f_0, is reflected in $\tilde{f}_s$ leading to frequency adaptation. An alternate solution can be achieved by adapting the number of samples used to construct each averaged sample for the comb filter. However, if the oversampling ratio (i.e., $\tilde{f}_s/f_s$) is small this adaptation will result in large frequency deviations in the sampling frequency. To see this, let us start with $\tilde{f}_s = l f_s$ and choose $l = 10$, that is, ten samples are averaged to construct one sample for the filter. Now adapting the number of samples will either require to average 9 or 11 samples. If the desired sampling frequency adaptation requires to average 9.5 samples, then the resulting error in frequency adaptation would be 5%. On the other hand, if the number of samples averaged for each filter sample is large, the achievable frequency adaptation resolution is improved; the resulting sampling frequency deviation is small. For $l > 50$, the frequency deviation error will be less than 1%.

IV. Performance Evaluation Results

The system parameters used for performance evaluation of the comb-filter-based compensator design are tabulated in Table I. To analyze the performance gains obtained using the comb filter, we compare its response with that of Butterworth and Chebyshev low-pass filters. For comparison, the required attenuation is fixed at 40 dB for each of the filters. To achieve an attenuation of 40 dB by using comb filter the parameter r needs to be at most 0.99, but we will use $r = 0.98$ for higher attenuation as well as smaller settling time. The order of the Chebyshev filter (N) to have an attenuation of 40 dB is 5 and that of Butterworth is 8 for a cutoff frequency of 120 Hz. Step responses of the three filters are shown in Fig. 8. It can be seen that the rise time of the comb filter is significantly better than the two low-pass filters. However, the settling time response of the filter is comparable with that of Butterworth filter and is better than that of Chebyshev filter. The phase response in Fig. 3(b) shows that, for parameter r close to unity, most of the frequency components have approximately zero-phase delay except the frequencies where the filter notches are present. This approximately zero phase delay, at most of the frequencies in the passband, is the reason for the comb filter step response starting with finite value, as shown in Fig. 8, in contrast to starting at zero for the two low-pass filters.

To see the closed loop performance, a load current with 5th, 7th, 11th, and 13th harmonics is drawn from the grid and the harmonic converter. The harmonic compensator is implemented to compensate for all the harmonics individually. For comparison, a Chebyshev low-pass filter of fifth order with passband and stopband frequencies of 60 and 120 Hz and with an attenuation of stopband equal to 40 dB is used. To see the performance improvement gained using the comb filter, we subject the HC to a load transient of 25% of the full load and observe the settling time improvement.

Fig. 9(a) shows the load transient response for the Chebyshev low-pass filter where the transient occurs at 0.15 s. Settling time is approximately equal to one line cycle for

TABLE I

System Parameters Used for Evaluation

Parameter name	Value
Phase voltage and frequency	120V, 60Hz
Load harmonic current, 5^{th}, 7^{th}	15A, 10A
Load harmonic current, 11^{th}, 13^{th}	4A, 2A
Normal load impedance	$R_l = 2\Omega$, $L_l = 5$mH
DC bus voltage and capacitance	50V, 2000μF
Filter sampling frequency, f_s	840 Hz
System sampling frequency, $\tilde{f}_s$	8400 Hz
Switching frequency	8400 Hz

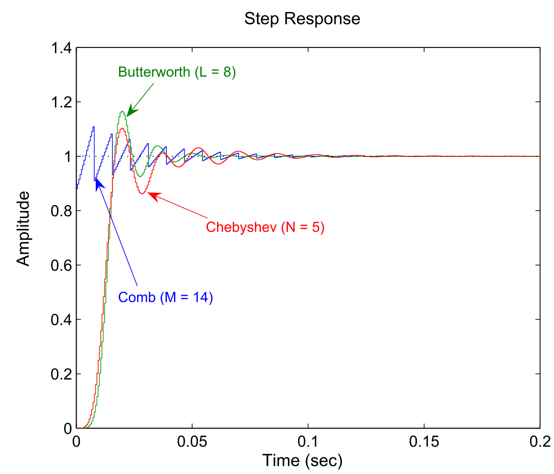

Fig. 8. Step response of the three filters. The response for the comb filter is obtained for $r = 0.98$.

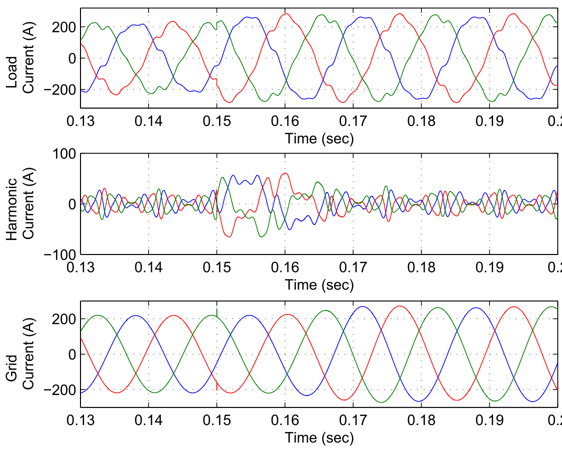

(a)

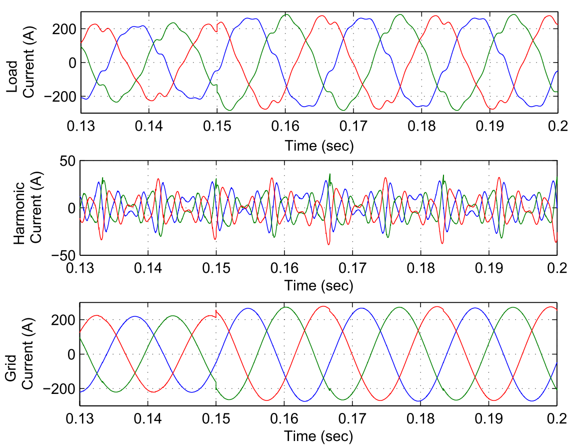

(b)

Fig. 9. Comparison of the load transient responses of (a) fifth-order low-pass (LP) Chebyshev filter having cutoff at 120 Hz and (b) comb filter with $r = 0.98$.

the low-pass filter and matches with the results provided in [9]. In case of comb filter, the settling time is approximately 1/100th of the line cycle as shown in Fig. 9(b). This result shows the significant performance gain in the transient response of the harmonic controller by using the comb filter compared with conventional low-pass filters.

To further elaborate the performance gains provided by the comb filter, the transient response in terms of d and q components of the load current is obtained and is shown in Fig. 10. Clearly, a faster dynamic response of the comb filter compared with the Chebyshev low-pass filter can be observed for the d component. Because the load transient was applied for active component at the fundamental frequency, we observe the transient in the d component of the current, but no transient appears in the q component. Furthermore, the nonzero value of the q component shows the reactive power compensation provided by the compensator.

Finally, we analyze the effect of the order of Chebyshev and comb filter on THD of the grid current. Fig. 11 shows that grid current THD increases as the filter order is reduced. It should be noted that the comb filter dynamic response will remain almost the same for different values of M owing to negligible phase delay in the filter passband. This is in contrast to the

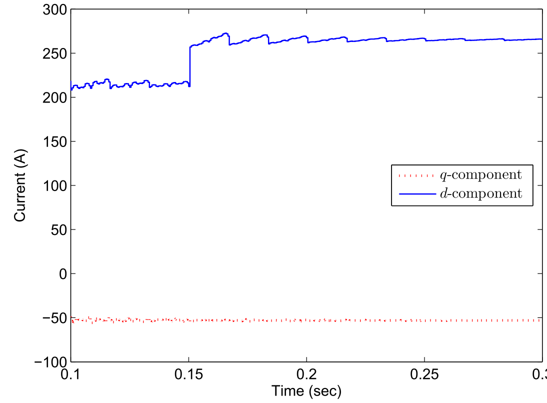

(a)

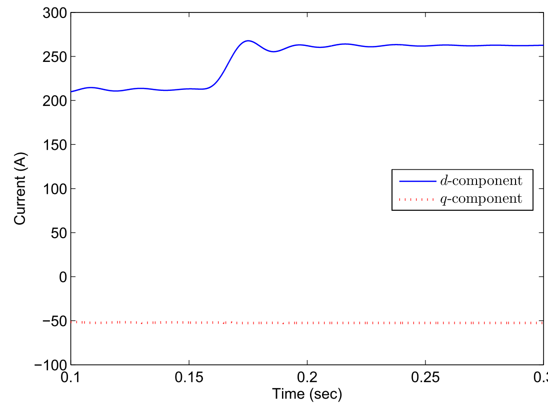

(b)

Fig. 10. Transient response for d and q components of the load current for (a) comb filter and (b) Chebyshev filter. These responses correspond to the fundamental frequency component.

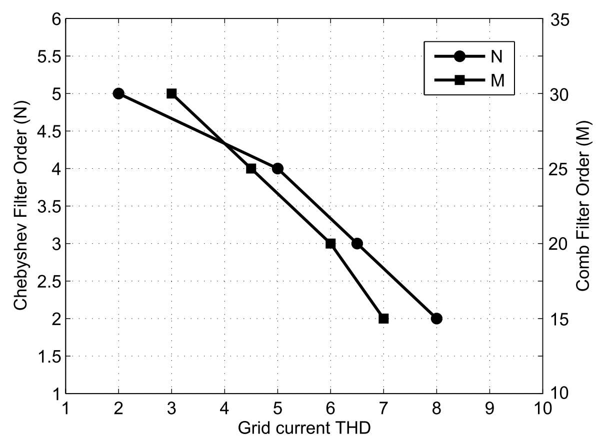

Fig. 11. Filter order requirements as a function of THD of the current drawn from grid.

Chebyshev filter whose dynamic performance degrades with an increase in the filter order owing to an increase in the phase delay. The implementation of the proposed digital comb filter solution requires less than 1 kB memory on the DSP, and the processing speed requirement is based on the desired sampling frequency.

V. Conclusion

An improved dynamic performance of synchronous frame harmonic as well as reactive power compensator can be obtained using the proposed comb-filter-based compensator design. Selective harmonic filtering can also be achieved by retaining the pole zero pairs at the frequency components to be filtered in the comb filter transfer function. However, the filter gain should be adjusted for normalized response. To make the proposed filter performance robust against any frequency variations, a sampling frequency adaptation-based mechanism is proposed. The sampling frequency adaptation along with comb filter coefficients adjustment in real time maintains the system performance under varying frequency conditions. The proposed solution can also be used for improving the dynamic response of a system by using a limited bandwidth compensator with selective unwanted frequency components.

References

[1] Y. Tang, P. C. Loh, P. Wang, F. H. Choo, F. Gao, and F. Blaabjerg, "Generalized design of high performance shunt active power filter with output LCL filter," *IEEE Trans. Ind. Electron.*, vol. 59, no. 3, pp. 1443–1452, Mar. 2012.

[2] J. Rocabert, A. Luna, F. Blaabjerg, and P. Rodriguez, "Control of power converters in AC microgrids," *IEEE Trans. Power Electron.*, vol. 27, no. 11, pp. 4734–4749, Nov. 2012.

[3] P. Mattavelli, "Synchronous-frame harmonic control for high-performance AC power supplies," *IEEE Trans. Ind. Appl.*, vol. 37, no. 3, pp. 864–872, May/Jun. 2001.

[4] M. Castilla, J. Miret, A. Camacho, J. Matas, and L. G. de Vicuña, "Reduction of current harmonic distortion in three-phase grid-connected photovoltaic inverters via resonant current control," *IEEE Trans. Ind. Electron.*, vol. 60, no. 4, pp. 1464–1472, Apr. 2013.

[5] M. Liserre, R. Teodorescu, and F. Blaabjerg, "Multiple harmonics control for three-phase grid converter systems with the use of PI-RES current controller in a rotating frame," *IEEE Trans. Power Electron.*, vol. 21, no. 3, pp. 836–841, May 2006.

[6] P. Rodríguez, A. Luna, I. Candela, R. Mujal, R. Teodorescu, and F. Blaabjerg, "Multiresonant frequency-locked loop for grid synchronization of power converters under distorted grid conditions," *IEEE Trans. Ind. Electron.*, vol. 58, no. 1, pp. 127–138, Jan. 2011.

[7] A. G. Yepes, F. D. Freijedo, J. Doval-Gandoy, O. Lopez, J. Malvar, and P. Fernandez-Comesana, "Effects of discretization methods on the performance of resonant controllers," *IEEE Trans. Power Electron.*, vol. 25, no. 7, pp. 1692–1712, Jul. 2010.

[8] L. Asiminoaei, E. Aeloiza, P. N. Enjeti, and F. Blaabjerg, "Shunt active-power-filter topology based on parallel interleaved inverters," *IEEE Trans. Ind. Electron.*, vol. 55, no. 3, pp. 1175–1189, Mar. 2008.

[9] L. Tolbert, F. Peng, and T. Habetler, "Dynamic performance and control of a multilevel universal power conditioner," in *Proc. IEEE IAS Annu. Meeting Ind. Appl. Conf.*, Oct. 1999, pp. 440–447.

[10] R. Grino, R. Cardoner, R. Costa-Castello, and E. Fossas, "Digital repetitive control of a three-phase four-wire shunt active filter," *IEEE Trans. Ind. Electron.*, vol. 54, no. 3, pp. 1495–1503, Jun. 2007.

[11] S. Rahmani, A. Hamadi, N. Mendalek, and K. Al-Haddad, "A new control technique for three-phase shunt hybrid power filter," *IEEE Trans. Ind. Electron.*, vol. 56, no. 8, pp. 2904–2915, Aug. 2009.

[12] Z. Shu, Y. Guo, and J. Lian, "Steady-state and dynamic study of active power filter with efficient FPGA-based control algorithm," *IEEE Trans. Ind. Electron.*, vol. 55, no. 4, pp. 1527–1536, Apr. 2008.

[13] J. Proakis and D. Manolakis, *Digital Signal Processing: Principles, Algorithms, and Applications*. Upper Saddle River, NJ, USA: Prentice-Hall, 1996.

[14] A. Prodic, J. Chen, D. Maksimovic, and R. Erickson, "Self-tuning digitally controlled low-harmonic rectifier having fast dynamic response," *IEEE Trans. Power Electron.*, vol. 18, no. 1, pp. 420–428, Jan. 2003.

[15] P. Zahradnik and M. Vlcek, "Analytical design method for optimal equiripple comb FIR filters," *IEEE Trans. Circuits Syst. II, Exp. Briefs*, vol. 52, no. 2, pp. 112–115, Feb. 2005.

[16] M. D. Kusljevic, "Simultaneous frequency and harmonic magnitude estimation using decoupled modules and multirate sampling," *IEEE Trans. Instrum. Meas.*, vol. 59, no. 4, pp. 954–962, Apr. 2010.

[17] J. Ren and M. Kezunovic, "Real-time power system frequency and phasors estimation using recursive wavelet transform," *IEEE Trans. Power Del.*, vol. 26, no. 3, pp. 1392–1402, Jun. 2011.

Muhammad Tahir (M'01) received the Ph.D. degree in electrical and computer engineering from the University of Illinois at Chicago (UIC), Chicago, IL, USA, in 2008.

He is currently an Associate Professor with the Department of Electrical Engineering, University of Engineering and Technology Lahore, Lahore, Pakistan, a Visiting Research Scholar with UIC, and a Principal Investigator on funded research projects related to air quality monitoring and intelligent camera networks. He has more than 30 international publications to his credit. His current research interests include wireless sensor networks, delay-tolerant networks, distributed resource optimization for wireless networks, and real-time wireless multimedia networks.

Dr. Tahir is a Reviewer of numerous IEEE journals and conferences.

Sudip K. Mazumder (S'97–M'01–SM'03) received the Ph.D. degree from the Department of Electrical and Computer Engineering, Virginia Polytechnic Institute and State University, Blacksburg, VA, USA, in 2001.

He has over 22 years of professional experience, and held research and development and design positions in the leading industrial organizations. He has served as a Technical Consultant for several industries. He is currently the Director of the Laboratory for Energy and Switching-Electronics Systems, and a Professor with the Department of Electrical and Computer Engineering, University of Illinois at Chicago (UIC), Chicago, IL, USA. He also serves as the President of NextWatt LLC, Hoffman Estates, IL, USA, a small business organization that he founded in 2008. He has authored over 160 refereed papers in prestigious journals and conferences, and published one book and eight book chapters. About 50% of his journal papers are published in the IEEE TRANSACTIONS with a current impact factor above 4. He has presented 56 invited/plenary/keynote presentations at leading organizations and institutions. His current research interests include interactive power electronics/power networks, smart grid, and energy storage, renewable and alternative energy-based power electronics systems for distributed generation and microgrid, and optically triggered widebandgap power electronics device and control technologies and SiC and GaN device-based high-frequency, high-temperature, and high-voltage power electronics. He holds eight issued and three pending patents.

Dr. Mazumder served as the first Editor-in-Chief of *Advances in Power Electronics* from 2006 to 2009, and the Guest Editor-in-Chief of the IEEE TRANSACTIONS ON POWER ELECTRONICS SPECIAL ISSUE ON HIGH-FREQUENCY-LINK POWER-CONVERSION SYSTEMS from 2013 to 2014. He currently serves as the Guest Coeditor of the *Special Issue on Sustainable Energy Systems Integration* published by the IEEE JOURNAL OF EMERGING AND SELECTED TOPICS IN POWER ELECTRONICS. He has also served as an Associate Editor of the IEEE TRANSACTIONS ON INDUSTRIAL INFORMATICS since 2014, the IEEE TRANSACTIONS ON POWER ELECTRONICS since 2009, the IEEE TRANSACTIONS ON INDUSTRIAL ELECTRONICS since 2003, and the IEEE TRANSACTIONS ON AEROSPACE AND ELECTRONICS SYSTEMS since 2008. He is also an Editorial Board Member of *Advances in Power Electronics*. He also served as an Associate Editor of the IEEE TRANSACTIONS ON CIRCUITS AND SYSTEMS and the IEEE POWER ELECTRONICS LETTER, and the Guest Co-Editor of the IEEE TRANSACTIONS ON POWER ELECTRONICS Special Issue on Power Electronics in DC Distribution Systems from 2011 to 2013 and the IEEE Special Issue on Advances in Power Electronics for Renewable Energy from 2010 to 2011. He is currently serving as the Plenary Chair of the 2015 IEEE Energy Conversion Congress and Exposition. He is also serving as the Technical Awards Committee Chair of the IEEE Power Electronics Society (PELS) Technical Committee on Sustainable Energy Systems (SES), the Chair of the IEEE PELS Subcommittee on Distributed Generation and Renewable Energy and the IEEE PELS Subcommittee on Power Semiconductors, a member of the IEEE PELS Standards Subcommittee, the IEEE Industrial Electronics Society (IES) Network Control Systems, and the IEEE IES Power Electronics Technical Committees. He served as the Chair of the Student/Industry Coordination Activities for the IEEE Energy Conversion Congress and Exposition, in 2010, a Steering Committee Member of the 2014 Power Electronics and Application Conference and Exposition, an Advisory Committee Member of the 2012 IEEE India International Conference on Power Electronics and the 2010 IEEE International Symposium on Power Electronics for Distributed Generation Systems, and served as the Co-Chair of SES. He has served as a Technical Program Committee Member of numerous IEEE sponsored and other reputed conferences, including the IEEE Energy Conversion Congress and Exposition, the IEEE Applied Power Electronics Conference and Exposition, the IEEE Industrial Electronics Conference, and the IEEE International Symposium on Power Electronics for Distributed Generation Systems. He was one of the five leading Researchers invited by the inaugural 2012 Clean Energy Trust Showcase, to deliver his vision on smart grid. From 2010 to 2011, he served as an Advisory Council Member of the Vice Chancellor for Research's Urban Resilience and Global Environment at UIC, and the Expert Representative on Smart Grid of UIC at the Midwestern Great Lakes Alliance for Sustainable Energy Research initiative, in 2009 and 2010. In 2008, he was invited by DOE to participate with several leading industries and selected academic professionals regarding high-millimeter-wave power converter for next-generation power grid, and by the NSF to participate in a unique workshop (comprising leading industries and research experts) leading to a decision on the nation's specific research and development focus on energy and energy distribution over the next 10 and 50 years. He has been invited to serve as the Working Group Committee Member of the IEEE P1676. In 2009, he was also part of the team that wrote the NSF and National Coordination Office for Networking and Information Report on Research Directions for Future Cyber-Physical Energy Systems. He has also served as a panel reviewer and a reviewer for NSF, DOE, ARPA-E, CRDF, and American Association for the Advancement of Science. He has received about 40 sponsored projects by the National Science Foundation (NSF), the Department of Energy (DOE), the Office of Naval Research (ONR), the Advanced Research Projects Agency-Energy (ARPA-E), the California Energy Commission, the Environmental Protection Agency, the Air Force Research Laboratory, the NASA, the Naval Sea Systems Command, and multiple leading industries in the above referenced areas, since joining UIC in 2001. He was a recipient of the Inventor of the Year Award at UIC in 2014, the University Illinois' University Scholar Award in 2013, the Teaching Recognition Program Award at UIC in 2011, the Prestigious Faculty Research Award from UIC for outstanding research performance and excellent scholarly activities in 2008 and 2006, respectively, the ONR Young Investigator Award and the NSF CAREER Awards in 2005 and 2003, respectively, the IEEE Prize Paper Awards in 2002, 2007, and 2013, respectively, and the IEEE International Future Energy Challenge Award in 2005.